Ionic Coulomb Blockade and the Determinants of Selectivity in the NaChBac Bacterial Sodium Channel

O. A. Fedorenko[a,b], I. Kh. Kaufman[c,d], W. A. T. Gibby[c], M. L. Barabash[c], D. G. Luchinsky[c,e], S. K. Roberts[a], P. V. E. McClintock[c,*]

[a] *Division of Biomedical and Life Sciences, Lancaster University, Lancaster, LA1 4YQ, UK*
[b] *School of Life Sciences, University of Nottingham, Nottingham, NG7 2UH, UK*
[c] *Department of Physics, Lancaster University, Lancaster, LA1 4YB, UK*
[d] *Deceased, 20 February 2019*
[e] *SGT, Inc., Greenbelt, MD, 20770, USA*

Abstract

Mutation-induced transformations of conductivity and selectivity in NaChBac bacterial channels are studied experimentally and interpreted within the framework of ionic Coulomb blockade (ICB), while also taking account of resonant quantised dehydration (QD) and site protonation. Site-directed mutagenesis and whole-cell patch-clamp experiments are used to investigate how the fixed charge Q_f at the selectivity filter (SF) affects both valence selectivity and same-charge selectivity. The new ICB/QD model predicts that increasing $|Q_f|$ should lead to a shift in selectivity sequences towards larger ion sizes, in agreement with the present experiments and with earlier work. Comparison of the model with experimental data leads to the introduction of an *effective charge* Q_f^* at the SF, which was found to differ between Aspartate and Glutamate charged rings, and also to depend on position within the SF. It is suggested that protonation of the residues within the restricted space of the SF is important in significantly reducing the effective charge of the EEEE ring. Values of Q_f^* derived from experiments on divalent blockade agree well with expectations based on the ICB/QD model and have led to the first demonstration of ICB oscillations in Ca^{2+} conduction as a function of the fixed charge. Preliminary studies of the dependence of Ca^{2+} conduction on pH are qualitatively consistent with the predictions of the model.

Keywords: `Ionic Coulomb blockade, Ion channel selectivity`, Voltage-gated sodium and calcium channels, Whole-cell patch clamp

1. Introduction

Biological ion channels provide for the highly-selective passive transport of physiologically important ions (e.g. Na^+, K^+ and Ca^{2+}) through the bilipid membranes of living cells. The channels consist of nanopores through complex proteins embedded in the membrane. Their selectivity for particular cations is determined by stochastic dynamics of the ions under the influence of powerful electric fields within a short and narrow selectivity filter (SF) carrying a binding site with fixed negative charge Q_f [1].

Following Eisenman [2], ionic selectivity arises through a balance between repulsion by the dehydration/self-energy barrier and electrostatic attraction/affinity to the binding site. It results in *resonant barrier-less conduction* for the selected ion [3–8], leading to selectivity phenomena such as divalent blockade of the sodium current [9, 10] and the anomalous mole fraction effect (AMFE) [10, 11] where the channel conductance is lower in a mixture of salts than in either of the pure salts at the same concentration.

Resonant barrier-less permeation can be described in terms of ionic Coulomb blockade (ICB) [12–14], a first-principles electrostatic phenomenon that appears in low-capacitance mesoscopic systems due to charge discreteness and an electrostatic exclusion principle [15–19]. ICB predicts Q_f to be an important determinant of selectivity, and one that is manifested strongly for divalent ions e.g. by giving rise to Ca^{2+} conduction bands [17]. ICB is closely similar to its electronic counterpart in quantum dots and nanostructures [20–23].

The basic ICB model for the permeation and selectivity of ion channels [14], has recently been enhanced [24, 25] by the introduction of shift/corrections to allow for the singular part of the ionic attraction to the binding site (i.e. local site-binding), bulk concentration, dehydration, and other sources of excess chemical potential $\Delta\mu$. The geometry- and concentration-dependent shift of the ICB

*Corresponding author
Email addresses: `fea80@ukr.net` (O. A. Fedorenko), `w.gibby@lancaster.ac.uk` (W. A. T. Gibby), `m.barabash@lancaster.ac.uk` (M. L. Barabash), `d.luchinsky@lancaster.ac.uk` (D. G. Luchinsky), `s.k.roberts@lancaster.ac.uk` (S. K. Roberts), `p.v.e.mcclintock@lancaster.ac.uk` (P. V. E. McClintock)

calcium resonant point resulting from these corrections provides a transparent explanation of the concentration dependence of the divalent (calcium) blockade threshold IC_{50} [26].

The voltage-gated bacterial sodium channels NaChBac, NavAb, NavMs, and NvsBa are a family of relatively simple channels with discovered structures that are widely used for studying the general features of conductivity and selectivity [27–35]. Site-directed mutagenesis, varying the fixed charge Q_f at the SF, is known to change their selectivity, switching sodium channels to calcium and *vice versa*. In turn, the alteration of Glutamate residues to similarly-charged Aspartate was also found to influence the channels' conductivity and selectivity [28–31]. The nature and physical origin of such transformations has remained unclear.

In this paper, we apply the ICB model to an analytic, numerical and experimental study of the effect of the fixed charge Q_f on the conductance and selectivity of NaChBac bacterial sodium channels and relevant mutants [26, 28, 31–33]. Using the picture of quantised dehydration (QD), we combine the idea of quantised (shell-based) dehydration with the balanced/shift-enhanced ICB model. A systematic mutation study of selectivity in the NaChBac channel shows that the resultant ICB/QD model accounts for the experimental Eisenman sequences and for measurements of divalent blockade in the mutants. Following Eisenberg [36], Zhang and Shklovski [37] and Aquilella-Arzo et al [38], we take account of the *effective charge* Q_f^* at a channel's binding site, which may differ from its nominal value Q_f^{nm} (equal to the arithmetic sum of charges on the isolated residues). This difference is hypothesised to be due to the protonation of closely adjacent residues in the EEEE or DDDD charged rings [9, 39–42].

2. Materials and methods

In what follows, with SI units, ε_0 is the permittivity of free space, e is the elementary charge, z is the ionic valence, k_B is Boltzmann's constant and T is the temperature. We use the conventional shorthand symbols for amino acid residues: Alanine (A); Aspartate (D, with $Q = -1|e|$); Glutamate (E, with $Q = -1|e|$); Leucine (L); Lysine (K, with $Q = +1|e|$); Serine (S); Threonine (T); Tryptophan (W); and so on, where the A, L, S, T and W residues are all uncharged.

2.1. Channels/mutants studied

The voltage-gated NaChBac bacterial channel [27, 28] is a tetrameric channel, whose SF is formed by 4 transmembrane segments each containing the six-amino-acid sequence LESWAS, corresponding to residues 190 — 195). This structure provides the highly-conserved {EEEE} locus E191 with a $Q_f^{nm} = -4e$ which is considered to create a single binding site for both mono- and divalent moving ions [27, 28]. Table 1 presents the set of channels generated and studied in the current research.

Mutant channels	Selectivity Filter Sequence 190	191	192	193	194	195	Q_f^{nm}/e
Wild type	L	E	S	W	A	S	-4
E191D	L	D	S	W	A	S	-4
E191A	L	A	S	W	A	S	0
S192K	L	E	K	W	A	S	0
S192E	L	E	E	W	A	S	-8
S192D	L	E	D	W	A	S	-8
E191D, S192E	L	D	E	W	A	S	-8
E191D, S192D	L	D	D	W	A	S	-8

Table 1: The wild-type NaChBac channel and its mutants studied in this paper, showing the amino acid sequences in their SFs and the corresponding nominal values of fixed charge Q_f^{nm}. The key SF positions (191,192) are shown in blue, except for changed residues which are highlighted in red. The mutants are grouped by their Q_f^{nm} values. Note that for the S192K mutant the neutral serine residue is replaced by a positively charged lysine which is expected to neutralise the negatively-charged side chain of the Glutamate resulting in a Q_f^{nm} value of 0.

2.2. Generation and expression of wild-type and mutant NaChBac channels

The NaChBac (GenBank accession number BAB05220) cDNA construct containing 274 amino acid residues was synthesised by EPOCH Life Science (www.epochlifescience.com) and subcloned into the mammalian cell expression vector pTracer-CMV2 (Invitrogen). Single amino acid mutations in the pore region of NaChBac were generated by site-directed mutagenesis using oligonucleotides containing the sequence for the desired amino acid substitutions (primers are listed in Supplementary Material Table S1) and Q5 Site-Directed Mutagenesis Kit (New England BioLabs Inc.). All mutations were confirmed by DNA sequencing. Wild-type NaChBac and mutant cDNAs were transiently transfected into CHO cells with TransIT-2020 (Mirus Bio). Transfected cells were identified by GFP fluorescence using an inverted fluorescence microscope (Nikon TE2000-s) and used for electrophysiological investigation 24—48 hours after transfection.

2.3. Electrophysiology

Whole-cell voltage clamp recordings were performed at room temperature (20°C) using an Axopatch 200A (Molecular Devices, Inc.) amplifier. Whole-cell currents were elicited by a series of step depolarizations (+95mV to -85mV in -15mV steps) from V_{hold} of -100mV. Details of the patch-clamp methods are presented in the Supplementary Material.

3. Models and theories

The features and mechanisms of electro-diffusive motion of ions through biological ion channels have been the

subject of numerous theoretical and simulation-based studies, performed with very different scales, models and methods [1, 43], including (in order of decreasing model detail) all-atom molecular dynamics (MD) simulations [4], mesoscopic Brownian dynamics (BD) simulations [43, 44], Monte-Carlo simulations [45], and Poisson-Nernst-Planck (PNP) simulations [46]. The different models represent different physical scales and provide complementary information. Simplified electrostatically-controlled and self-consistent BD models have already shown their utility for describing relatively wide calcium/sodium channels [3, 16, 18, 44, 45].

3.1. Self-consistent electrostatic and Brownian dynamics model

A simple electrostatic/BD model (Supplementary Material, Fig. S5) is used to describe the SFs of calcium/sodium ion channels. It treats the channel's SF as a water-filled, cylindrical, negatively-charged pore in the protein, radius $R \approx 0.3$nm and length $L \approx 1$nm.

3.2. Ionic Coulomb blockade

ICB is a fundamental electrostatic phenomenon that emerges in the electro-diffusive transport of ions through narrow, low-capacitance channels, whether biological [13–15] or artificial [12, 23]. ICB claims that for $z > 1$ (e.g. for Ca^{2+}) the current I *vs.* Q_f exhibits *Coulomb blockade oscillations* (multi-ion conduction bands [17]) between zero-conduction blockade points $Z_n = -zne$ at one extreme, and resonant $M_n = -ze(n + 1/2)$ points with barrier-less permeation at the other, where the index n is equal to the number of ions captured at the SF. The oscillations in I correspond to a *Coulomb staircase* in the channel/SF occupancy P_c (see Supplementary Material, Fig. S6); the resonant points M_n correspond to the $n \to n+1$ transition in P_c.

For completeness, and for convenience of the reader, the Supplementary Material provides a brief summary of the ICB model [13, 26, 47]. A brief description of ICB is also presented in Wikipedia
https://en.wikipedia.org/wiki/Ionic_Coulomb_blockade.

3.3. Resonant quantised dehydration model

Dehydration, either full or partial, is thought to be the main source of selectivity between equally charged ions, e.g. monovalent alkali metal ions [3, 46, 48, 49]. The basic ICB model takes account of hydration/dehydration only through the dielectric self-energy U_q^{SE} in a 1D Coulomb approximation [3, 16] which is independent of the size of the ion, so additional effects need to be included in the model.

One such effect is the discreteness of the hydration shells, which strongly influences selectivity [3, 7, 8, 50]. Zwolak *et al.* [50] have suggested a simple model of QD energetics based on consideration of hydration shells as thin spherical layers, calculation of the hydration energies of Born shells, and summation over shells.

We combine Zwolak's model with ICB, yielding the ICB/QD model which predicts that, for moderately wide ($R_c \approx 0.3$nm) Ca^{2+}/Na^+ channels, the growth of $|Q_f|$ leads to a shift of Eisenman sequences toward larger ions, i.e. $Na^+ \to K^+$. This result arises from an increase in dehydration energy with growth of R_{ion} (see Supportimg Material Fig. S7). That is the main result of the ICB/QD model that will be tested experimentally here. In contrast, the narrower ($R_c \approx 0.2$nm) KcsA potassium channel demonstrates an inverse $K^+ \to Na^+$ shift with growth in field strength [2].

The model is described in the Supplementary Material.

3.4. Protonation of EEEE/DDDD charged rings

Protonation of charged residues is to be anticipated in the confined space within the SF. Possible protonation of the EEEE locus has been under consideration for many years [18, 39, 46] and the present results can be construed as additional evidence in favour of this hypothesis. Note that Boiteux *et al* [51] have recently discussed possible alternative explanations for Na^+ selectivity in sodium channels.

The proposed protonation model is described in the Supplementary Material.

4. Results and discussion

We perform an experimental study of mutation-induced transformations of conductivity and selectivity in NaChBac voltage-gated bacterial channels, including both Q_f-varying mutations and Q_f-conserved (D⇌E) substitutions within the SF, in order to see whether the results could be understood within the framework of the ICB model. Increasing the value of $|Q_f|$ was expected [13, 26] to lead to:

- A resonant variation of the divalent current with Q_f (ICB oscillations)
- Stronger divalent blockade of the Na^+ current, following the Langmuir isotherm.

Previous mutant studies [27–29, 31] investigated a limited number of possible (D,E) combinations in the key positions 191 and 192. Our present systematic study of the possible mutants L{ES/DS/EE/ED/DE/DD}WAS enables us to identify the influences of both Q_f^{nm} and of the D/E substitutions in positions 191 and 192, as illustrated in Table 1. We will present selectivity sequences for monovalent and divalent ions, recorded for the mutants listed above, with Q_f^{nm} varied in the range $0e$ to $-8e$, and with the permutations of D and E shown in Table 1. We have also made divalent blockade measurements, providing us with the experimental information needed for application of the extended ICB model (see below) incorporating the effect of QD.

Note that whole-cell currents were used to determine the cation permeability and selectivity sequences shown in

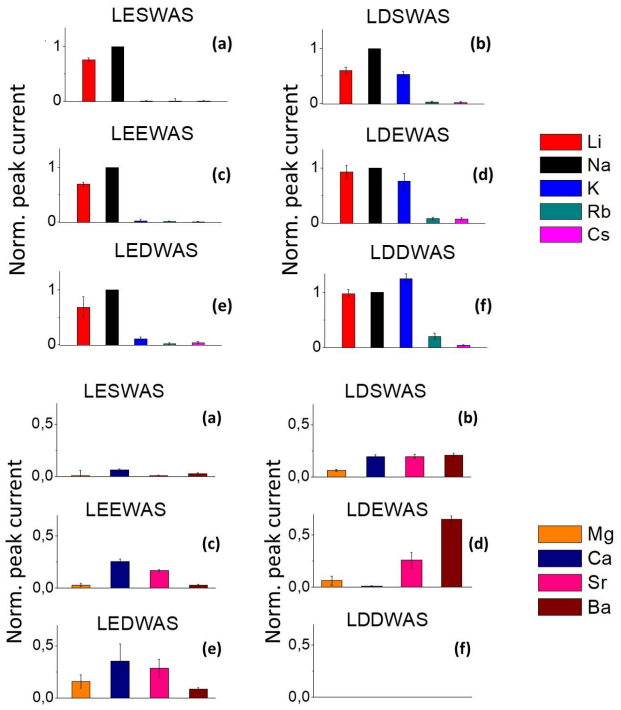

Figure 1: Experimental cation permeabilities. Upper panel: monovalent cation permeabilities, for Na^+, Li^+, K^+, Rb^+ and Cs^+ (as labelled). Lower panel: divalent cation permeabilities, for Mg^{2+}, Ca^{2+}, Sr^{2+} and Ba^{2+} (as labelled). Note that no divalent current could be measured for LDDWAS. In each panel the peak inward current densities $I_{\rm peak}$ are shown for: (a) LESWAS (wild type NaChBac) with $Q_f^{nm} = -4e$ and the mutant (b) LDSWAS also with $Q_f^{nm} = -4e$; and for four mutants (c) LEEWAS, (d) LDEWAS, (e) LEDWAS, and (f) LDDWAS each with $Q_f^{nm} = -8e$. In each case, normalised peak inward current magnitudes were recorded from the same cell in a Na^+ bath solution prior to replacement of extracellular Na^+ by the test cation. Averages (±Standard error of mean) are from at least 5 cells. For I–V relationships of the presented data see Fig. S3 in the Supplementary Material.

Figure 1. Whole-cell currents are the product of number of channels, open probability and single channel current amplitude. Thus the whole-cell current densities for different mutants can result from a wide range of factors, including some which do not reflect ion conductance through the channel pore (e.g. Yue et *al.* [28] report different expression levels for NaChBac mutants in CHO and COS-7 cells). In an attempt to exclude those effects unrelated to ion permeation, we report cation conductance normalised to sodium currents (details below and in the caption of figure 1), a procedure which is in line with previous reports on ion channel permeability [27–29, 52]. However, for completeness, the Na^+ current density for each of the mutants used in the current study is shown in Figure S0.

4.1. Ionic conductance for zero-charge mutants

The ICB model predicts that, for an uncharged pore ($Q_f = 0$), the self-energy barrier U_q^{SE} should prevent conduction of any kind of ions. This condition corresponds to the ICB blockaded point Z_0 [13].

In the experiments, the two mutations E191A (generating LASWAS) and S192K (generating LEKWAS) were used to produce two different NaChBac mutants, each with Q_f=0. They exhibited no measurable conduction of either monovalent nor of divalent cations (see Supplementary Material Fig. S2.), consistent with the ICB model. The model predicts stronger current suppression for divalent than for monovalent ions, but this distinction was below the sensitivity of our measurements and could not be tested.

Similar ICB-driven blockade was recently observed in uncharged artificial sub-nm MoS_2 nanopores, where a voltage/energy gap was found corresponding to zero ionic current for both mono- and divalent ions when the voltage across the nanopore was small[23].

4.2. Monovalent selectivity sequences of charged mutants

Earlier studies of the E191D mutation in NaChBac [29, 30] (or, equivalently, E178D mutations in NavMs [31] and *vice versa*) have shown that the E⇌D substitution in this key position leads to a significant change in selectivity features even though there is no change of the nominal charge. The mutation E191D leads to the emergence of K^+ conduction and to a general shift of monovalent selectivity sequences toward larger ions[30]. A similar selectivity $Na^+ \rightarrow K^+$ shift was recorded for the E178D mutation in the NavMs channel [31], the E→D-related selectivity shift was also observed for the NsvBa (LDSWGS) channel [29]

Fig. 1 upper panel) presents the results of our own systematic study of the influence on monovalent ionic selectivity of E⇌D alterations at positions 191 and 192. The peak conductivities for (a) wild type NaChBac LESWAS and for the five mutants (b)-(f) as labelled were determined by normalising peak current magnitudes *from the same cell* recorded in a bath solution first of Na^+, prior to replacement of the Na^+ by the test cation Li^+, K^+, Rb^+ or Cs^+ as indicated (thus representing cation influx relative to Na^+ influx).

Fig. 1 (upper panel) can be thought of as a "response matrix" in a Design of Experiment sense [53]. The different columns correspond to E⇌D residues alteration at position 191: E191 for the left column and D191 for the right column. The different rows correspond to S⇌E⇌D residues alteration in position 192. The first row {(a), (b)} represents the singly-charged mutants LESWAS, LDSWAS, while the other two rows represent a 2×2 submatrix of the nominally doubly-charged mutants LEEWAS/LDEWAS /LDEWAS/LDDWAS. Supplementary Material Figs. S3 and S0 show the original *I–V* characteristics and representative currents, respectively, for monovalent conductance.

The columns of Fig. 1 (upper panel) present a comparison of the D191 mutants (left) with their E191 counterparts (right); results confirm that the residue in position 191 is the main determinant of monovalent selectivity in NaChBac mutants: the E191D mutation provides a significant shift towards favouring the influx of larger monovalent cations. Note that the NaK channel, possessing a

similar DDDD charged ring at the SF, is also Na^+/K^+ non-selective [54]. Plots {(c),(d),(e),(f)} also show that additional E192D mutations lead to a relatively weak extra shift in the same direction.

Now we consider these phenomena in more detail.

- LESWAS, LEEWAS, LEDWAS. All mutants having an E191 residue present Na^+-centred Eisenman sequences, whereas increasing the nominal total charge from $|Q_f^{nm}| = 4e$ for LESWAS to $|Q_f^{nm}| = 8e$ for LEEWAS and LEDWAS leads only to a weak increase of K^+ permeability.
- LDSWAS, LDEWAS, LDDWAS. The D191 mutants have Eisenman sequences shifted toward favouring K^+, and the difference in Q_f values leads to weak additional permeability of large-sized ions in the LDEWAS and LDDWAS mutants which have larger $|Q_f^{nm}|$. This double-D LDDWAS mutant exhibits an increased shift.

The observed shift of monovalent selectivity towards larger ions can be explained by the ICB/QD model (see Sec. S3.3, Fig. S7 (a),(b)), on the assumption that the E191D mutation leads to a significant increase in the effective charge $|Q_f^*|$, whereas further mutation of position 192 to a D (from an S or E) provides only a minor increase of $|Q_f^*|$. We will connect the relative sizes of the increase in $|Q_f^*|$ to smaller protonation of the DDDD ring in comparison with EEEE [39].

4.3. Divalent selectivity sequences of charged mutants

Fig. 1 (lower panel) presents divalent cation permeabilities for the mutants studied. The peak conductivities for (a) wild type NaChBac LESWAS and for the mutant channels (b)-(e) are shown for the cations Mg^{2+}, Ca^{2+}, Sr^{2+} and Ba^{2+} (as labelled). As in the case of monovalent cations, they were normalised to the peak current recorded in Na^+ bath solution. No conduction of any divalent ion could be recorded for LDDWAS (Supplementary Material Fig. S4). Similarly to the monovalent case, Fig. 1 (lower panel) can be thought as a "mutation matrix" for divalent conduction.

Whereas the wild-type LESWAS channel exhibits little divalent cation permeability, in agreement with Yue *et al* [28] and Guardiani *et al* [33], most of the mutants show some calcium conductivity. Although less pronounced, the divalent selectivity sequences demonstrate a shift toward larger ions for both the E191D and S192D mutations. Thus the LEEWAS and LEDWAS mutants show maximal permeability for Ca^{2+} ions, whereas the LDSWAS and LDEWAS mutants are more Ba^{2+}-permeable. Although there are no comparable previous studies that systematically test divalent cation permeability of equivalent bacterial sodium channel mutants, it is noteworthy that the E178D mutant (equivalent to E191D in the present student study) of another bacterial sodium channel, NsvBA, also reports comparable permeability for Ba^{2+}. Furthermore, consistent with the relative divalent conductances shown for the LDSWAS mutant in Figure 1, the equivalent E to D substitution in the selectivity filter of the NsvBa channel results in a relative permeability sequence of $Ba^{2+} = Sr^{2+} = Ca^{2+} \gg Mg^{2+}$ [29]. Note also that Wang *et al.* [55] reported that the LDSWAS mutation of NaChBac has a significant impact on organic cation binding in the pore and is thus consistent with LDSWAS and LESWAS having distinct cation permeabilities.

Remarkably, both wild-type LESWAS ($Q_f^{nm} = -4e$) and the doubly-charged ($Q_f^{nm} = -8e$) LDEWAS and LDDWAS mutants show strong blockade of divalent Ca^{2+} ions, but maintain conductance for small monovalent ions (Na^+). We connect these observations with the above-mentioned growth of $|Q_f^*|$ for the E191D, S192E and S192D mutations, and corresponding selectivity shift, in accord with the ICB/QD model (see Sec. S3.3, Fig. S7(c),(d)). The resultant conductance oscillations have ICB blockade points Z_n of different-order, with smaller n_1 for LESWAS and larger $n_2 > n_1$ for LDEWAS. The exact values of n_1 and n_2 will be discussed below. Note that the absence of measurable divalent current for LDDWAS is attributable to high affinity blockade of the channel by Ca^{2+} [56] as illustrated in Fig. 2 and is consistent with the results previously reported by Tang et al. (2014) [52] for the equivalent mutation in NavAb.

4.4. Divalent blockade of Na^+ current and Q_f^* mapping

Divalent blockade is a phenomenon of a strong attenuation of a monovalent (e.g. Na^+) current I_{Na} by micromolar extracellular concentrations of divalent (e.g. Ca^{2+}) ions $[Ca^{2+}]$, manifesting a characteristic S-shaped dependence of I_{Na} on $\log[Ca^{2+}]$. The phenomenon has been well-documented in calcium channels [10, 46, 57]. Divalent blockade appears on account of the stronger affinity of the divalent ions to the binding site, so that the measurement of the divalent blockade threshold IC_{50} provides a sensitive tool of evaluating this affinity. We use it as a tool to introduce an effective value of the fixed charge Q_f^* (see below).

The ICB model predicts the Langmuir isotherm/Fermi-Dirac shape of I_{Na} *vs.* $\log[Ca^{2+}]$ [13, 26] which is known to be consistent with typical shape of attenuation curves [58, 59]. The ICB model also predicts a linear dependence of the blockade threshold/affinity $\log IC_{50}$ on the effective charge Q_f^* [13, 26]:

$$\ln(IC_{50}) = b_Q \frac{Q_f^* - M_0}{e}; \quad b_Q = \frac{E_s}{z k_B T};$$
$$E_s = \frac{z^2 e^2}{2C_s} = \frac{\lambda_B L_c}{2R_c^2} k_B T \qquad (1)$$

where $M_0 = ze/2$, $\lambda_B \approx 0.7$nm is the Bjerrum length [16], and $b_Q \approx 10$ (for model NaChBac channel having $R_c = 0.3$nm, $L_c = 1$nm and the self-energy $E_s = 20 k_B T$), is a valence- and geometry-dependent coefficient (used as fitting parameters). We cannot quantify these constants *a priori*, and we will use the ICB singular points Z_n to invert Eq. (1) and restore the map of Q_f^* *vs* $\ln IC_{50}$.

Fig. 2 (a) shows the results of divalent blockade experiments for NaChBac channels/mutants with $Q_f^{nm} = -4e$ and $Q_f^{nm} = -8e$. Bath solutions containing mixtures of Na^+ and Ca^{2+} in varying concentrations were used to investigate divalent blockade and the possibility of AMFE on both the whole-cell current magnitude and current reversal voltages. The experiments started in a bath solution with 140 mM Na^+ and 10 nM of $[Ca^{2+}]_{free}$, which was sequentially replaced by solutions containing increasing addition of Ca^{2+} at concentrations up to 1 mM $[Ca^{2+}]_{free}$, followed by solution in which Na^+ was replaced by Ca^{2+} up to 28.7 mM of $[Ca^{2+}]_{free}$ (see details in Table S3).

The LESWAS (WT) channel does not exhibit any Ca^{2+}-dependent block of the Na^+ influx [26, 33], and thus the reduced current results from extracellular Na^+ being replaced with equimolar Ca^{2+} and represents the effect of substrate depletion. All other mutants show divalent blockade with systematically changing IC_{50}: it decreases by the E191D, S192E and E192D mutations. The attenuation curves $I(Na)$ *vs.* $\log[Ca]$ for different mutants are generally parallel each to other, in accordance with the ICB-model [26].

The LDSWAS mutant shows weak divalent blockade of the Na^+ current with $IC_{50} \approx$1mM. The LEDWAS and LEEWAS mutants exhibit $IC_{50} \simeq 10\mu$M, with LEDWAS showing an additional weak shift relative to LEEWAS. The LDEWAS and LDDWAS Ca^{2+} blockade plots were further shifted toward lower concentrations relatively to the E191 mutants. Thus, (i) the D residue provides stronger site affinity than an E in the same position, but (ii) the difference between D and E is significant for the E191D mutation, but is only minor for the E192D mutation, similar to the differences in selectivity measurements(see Fig. 1).

As mentioned above, the notion of *effective charge* Q_f^* for ion channels was introduced [18, 36, 37] as a fitting parameter. We now propose a Q_f^* mapping (i.e. an estimation of Q_f^* for all the mutants studied) on the basis of the affinity and positions of the ICB singular points.

Fig. 2(b) presents the inversion of Eq. 1, based on reference points $Z_1 = -2e$ and $Z_2 = -4e$, and using the IC_{50} data of Fig. 2(a) to map Q_f^* for mutants, intermediate between the Z_1 and Z_2. To do so we rewrite (1) in the Newton's interpolation form:

$$Q_f^* = Z_1 + \frac{e}{b_Q}\left(\ln\left(IC_{50}\right) - X_1\right);$$
$$b_Q = e\frac{X_2 - X_1}{Z_2 - Z_1} = \frac{X_2 - X_1}{z}; \qquad (2)$$

where $X_i = \ln\left(IC_{50}\left(Z_i\right)\right)$. The results presented here lead to an estimate of $b_Q \approx 5$, which is reasonably close to the *a priori* modelled value, and corresponds well to a shorter SF: $L_c \approx 0.5$nm. The full results of the mapping are presented in Table S5.

An important feature of the ICB model is that it provides a natural explanation for the strong selectivity of

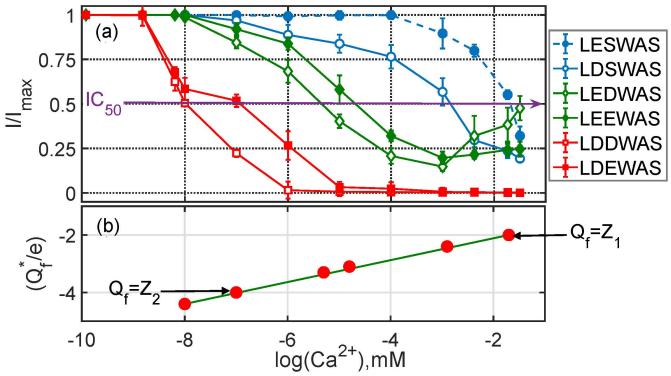

Figure 2: Divalent blockade and effective fixed charge Q_f^* map in NaChBac mutants with $Q_f^{nm} = -4e$ (LESWAS, LDWAS) and $Q_f^{nm} = -8e$ (LEEWAS, LEDWAS, LEDWAS and LDDWAS) (indicated in inset). (a) The relationships of the averaged normalized peak currents I/I_{max} *vs.* $\log[Ca^{2+}]$ are plotted for increasing Ca^{2+} content, ranging from 0.1 nM to 30 mM with Na^+ substitution. The line marked IC_{50} shows the cross-section at $I/I_{max} = 0.5$, i.e. Ca^{2+} affinity. (b) Q_f^* vs IC_{50} map, based on (a), reference points $Z_1 = -2e$ and $Z_2 = -4e$ are shown.

particular channels (i.e. those having particular values of Q_f) through their identification/mapping onto particular singular ICB points. Ideally, a channel should be in a near–to–resonant M_n state for the conducted ion, while in a blocking Z_n state for the non-conducted ion. This scheme works particularly well for Ca^{2+}/Na^+ valence selectivity because of the strong ICB effects observed for Ca^{2+} ions.

The resultant mapping was defined as follows (see Table S5 and Fig. 2(b)):

- LASWAS. Uncharged mutants do not conduct any ions, which behaviour corresponds to the $Z_0 = 0$ ICB point. Similar Z_0-type electrostatic blockade was observed experimentally in MoS_2 nanopores where it was used as an evidence of ICB [23].
- LESWAS. The wild-type NaChBac channel conducts Na^+ ions but does not conduct Ca^{2+} ions. Hence, in the ICB model, it must correspond to one of Ca^{2+} stop bands Z_n. We infer that $Q_f^* = Z_1 = -2e$. That is the first Q_f^* mapping reference point. In our model, the NaChBac channel apparently possesses an effective value $|Q_f^*| < |Q_f^{nm}|$ significantly lower than was believed previously [28, 30] and well-correlated with protonation model. The alternative inference $Q_f^* = Z_2 = -4e$ is not consistent with the experimental observation that LESWAS channel demonstrates *lower* Ca^{2+} affinity than the LDSWAS mutant.
- LDEWAS. Experimentally, this mutant does not conduct Ca^{2+} ions, so we assume it to be close to the next (after Z_1 for LESWAS) Ca^{2+} Coulomb blockade point $Q_f^* = Z_2 = -4e$. This point is used as the second mapping reference point.
- LDSWAS, LEEWAS and LEDWAS are calcium-conductive "intermediate" mutants. We infer that their Q_f^* val-

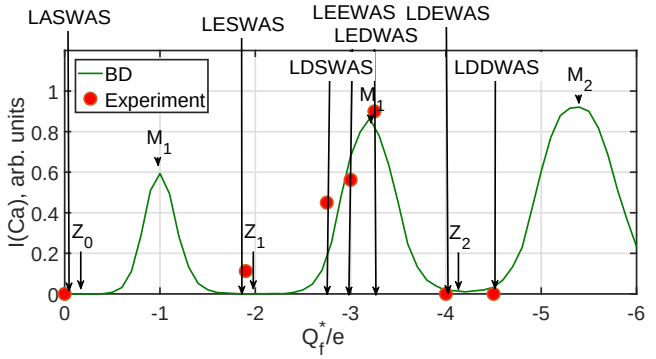

Figure 3: BD-simulated (green line) and experimental (red circles) multi-ion Ca^{2+} conduction bands / ionic Coulomb blockade oscillations *vs* the effective fixed charge Q_f^*. The conduction bands in the Ca^{2+} current I were simulated for a pure bath with $[Ca^{2+}]$=160 mM. Experimental conductance data are taken from Fig. 1. The Q_f^* positions of the various NaChBac mutants having $Q_f^{nm} = 0$ (LASWAS), $Q_f^{nm} = -4e$ (LESWAS, LDSWAS), $Q_f^{nm} = -8e$ (LEEWAS, LEDWAS, LDEWAS, LDDWAS), calculated by fitting Eq. 1 to AMFE data, are indicated.

ues are proportional to IC_{50} in each case, in accordance with Eq. 1 and with Fig. 2(a),(b).

- LDDWAS was mapped to $Q_f^* \approx -4.4e$ using the appropriate IC_{50} value.

Fig. 3 presents ICB oscillations based on the putative Q_f^* map, determined as described above, for the site-directed mutants of NaChBac. Experimental data (taken from Fig. 1) are superimposed on the multi-ion Ca^{2+} conduction bands found in BD simulations. The vertical arrows indicate site-directed mutants with their respective effective fixed charges Q_f^* deduced by the method described above. The model used for the BD simulations takes no account of the QD corrections, so that the overall agreement with experiment should be considered as preliminary.

Fig. 3 represents the first experimental evidence for ICB oscillations of Ca^{2+} conduction in biological ion channels. The oscillations manifest themselves strongly at room temperature, unlike their electronic counterpart in quantum dots which become significant only at low temperatures [20]. We emphasise that Q_f^* constitutes the main determinant of selectivity, in agreement with the ICB/QD model.

Supplementary Material Fig. S8 presents in diagrammatic form the quasi-periodic sequence of multi-ion blockade/conduction modes arising from growth of $\{n\}$ as Q_f^* increases, together with putative identifications of particular modes and of the NaChBac mutants used in this work. The diagram is based on the data shown in Table. S5 and Fig. 3.

4.5. Protonation as the putative origin of Q_f^*

The negative fixed charge Q_f of bacterial channels and their mutants is provided by the ionised side chains of the Aspartate (D) and Glutamate (E) residues, which are the only negatively-charged protein side chains. They are characterised by their iso-electric point pK_a which is the value of the hydrogen index pH providing an ionisation of 0.5, equivalent to zero net charge on the residue. Glutamates and Aspartates have the same nominal charge ($Q_f^{nm} = -1$) and very similar $pK_a \approx 4$, but different lengths of side chain, resulting in the the EEEE-ring exhibiting a different arrangement of side chains compared to that for the DDDD-ring [56]. This structural difference can lead to different (and potentially opposite) effects: due to the difference in local binding and to the difference in protonation and hence in the effective fixed charge Q_f^*.

We hypothesize that protonation is the dominant effect and that the increase of affinity corresponding to the E191D mutation is defined by significant protonation of the relatively small-radius EEEE charged ring due to overlapping of the electron and proton clouds between neighbouring residues in the ring: such effects have been studied by Furini *et al* [42]. Similar effects on the pK_a and protonation state of Glutamate, also due to space restriction, were calculated for the narrower KcsA channel, where pK_a was shifted to $pK_a = 9.2$ [60]. The effect of Glutamate to Aspartate substitution on EEEE protonation in Ca^{2+} channels was studied by Chen and Tsien [39]. In contrast, the DDDD ring could be more ionized at physiological pH, coming closer to the full ionization of free residues. Note that the protonation-based interpretation implies that the effective Q_f^* value is not an averaged "conceptual value" but, rather, that it reflects the "true" electrostatic value of Q_f, differing from the nominal value Q_f^{nm} corresponding to Q_f for an isolated residue.

Details of the protonation model are presented in the Supplementary Material.

4.6. Preliminary study of pH dependence of Ca^{2+} conductance

With protonation included, the ICB model predicts a strong dependence of Ca^{2+} conductance on the pH of the external solution. It had been shown previously that the pH can alter dramatically the Na^+ conductance for NaChBac [29] and Na^+/K^+ selectivity [30]; there are, however, no data related to the dependence of the Ca^{2+} selectivity on pH.

Fig. 4 presents the results of our preliminary study of the effect of variations in extracellular pH on Ca^{2+} conductance in the LESWAS and LDSWAS NaChBac channels. The results are strongly influenced by the residue type at position 191. Panel (e) shows that the inward Ca^{2+} current for wild type LESWAS was small and relatively insensitive to pH changes. Note that absolute values (pA/pF) of currents are used: the points in each given plot relate to the same mutant so that normalisation is unnecessary.

Such behaviour corresponds to the position of LESWAS on the ICB conduction *vs.* Q_f^* map (Fig. 3), i.e. to the Ca^{2+} stop band for all pH, thus confirming our interpretation of LESWAS as lying at the Ca^{2+} blockade point. Panel (f) for the LDSWAS mutant demonstrates a significant calcium current I, decreasing with growth of pH (and Q_f^*),

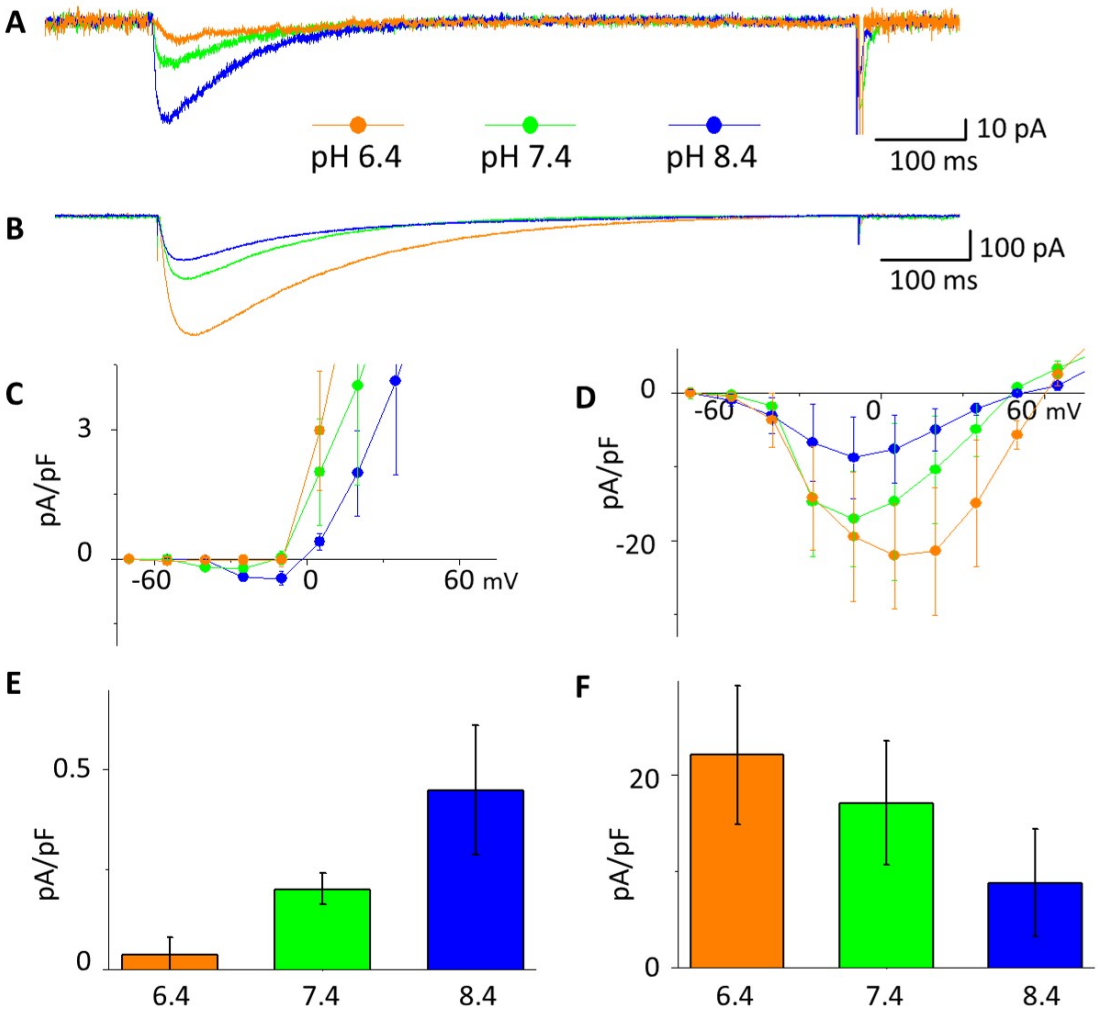

Figure 4: Effect of extracellular pH on Ca^{2+} currents from the NaChBac channels LESWAS (A, C, E) and LDSWAS (B, D, F). Plots A and B show original whole-cell currents from cells in response to a depolarising step to -10 mV (from $V_{\text{hold}} = -100\,\text{mV}$) in a standard bath solution (SBS) containing 100 mM Ca^{2+} at pH 6.4 (yellow), 7.4 (green) and 8.4 (blue). Plots C and D show the mean current-voltage relationships ± the standard error of the mean (SEM) for the whole-cell currents plotted in A and B. Plots E and F show the peak current densities obtained from the current-voltage relationships shown in parts C and D.

which corresponds to the decreasing-slope side of the ICB oscillation I *vs* Q_f^*. Such behaviour seems to be inconsistent with our mapping (Fig. 3) in which the LDSWAS "working point" is located on the increasing-slope side. Another question, arising in connection with protonation, is possible dependence of Q_f^* on existance of capured ion. Further investigation should be performed to understand these patterns.

We note that, regardless of the mapping, the effects of pH change on the currents for LESWAS and LDSWAS are distinct, and are consistent with the protonation state of the side chains being an important factor in determining Q_f^*.

4.7. Comparison with molecular dynamics simulations

Some of the NaChBac conduction data used here have also been discussed and analysed with the illumination of MD simulations [32, 33, 56]. The MD approach uses a combination of equilibrium simulations, Markov state modelling and meta-dynamics to show that Na^+ permeation in NaChBac occurs through a knock-on mechanism involving two or three ions. The MD results are validated by the consistency between single channel current measurements and the currents predicted by equilibrium simulations using linear response theory. They are also in agreement with works on the homologous NavAb channel [61]. Guardiani *et al* [32] show that the number of Na^+ or Ca^{2+} ions occupying the SF of NaChBac during the MD simulations can be fully justified on the grounds of the ICB model, and that aspartates and glutamates play different roles [56]. In particular, the ICB model is in agreement with MD simulations showing that the 3rd Na^+ ion can occupy the SF only in a transient way to trigger the knock-on mechanism or to be bounced back into the bulk;

see also the Supplementary Discussion of Guardiani *et al.* [56]. Thus for wild type NaChBac the results from the ICB model, the MD simulations, the BD simulations, and the experiments are all mutually consistent.

The recent paper by Wang *et al* [55] adds valuable insight, in that it confirms that the acidic side chains offer a flexible binding site that is exposed to the aqueous solution. Thus it is consistent with the present manuscript in proposing possible differential protonation and hence non-equivalence of the charge associated with the E and D residues at this position in the pore.

Further research will be needed to provide a full reconciliation of the ICB/QD and MD-based conduction and selectivity models for the mutants of NaChBac.

5. Conclusions

Our mutation study of conductance and selectivity in NaChBac-based channel/mutants has revealed that the E191D mutation provides a strong shift of monovalent and divalent selectivity sequences toward larger ion sizes, together with a corresponding reduction in IC_{50} for Ca^{2+} blockade of the Na^+ current. Interpreted within the framework of the ICB/QD model, these results lead to the introduction of an effective value Q_f^* of the fixed charge as the determinant of ionic selectivity: Q_f^* was interpreted in terms of a protonation model, and its value was found to be significantly smaller than the nominal fixed charge Q_f^{nm}. The main results are as follows:

1. Our new ICB/QD model predicts that increasing $|Q_f^*|$ leads to a shift of the Eisenman selectivity sequences toward ions with larger radii, for both monovalent and divalent cations, an effect that is opposite to the original Eisenman-claimed shift in the narrower KcsA channel. The experiments confirmed that the shifts predicted by the model do occur in reality.
2. The charge-varied mutants exhibit divalent blockade of Na^+ current by small amounts of Ca^{2+}. Mutants with the same Q_f^{nm} (-4 or -8), generated with different combinations of Glutamate and Aspartate at the SF, exhibit markedly different cation permeation profiles and hence have different effective charge Q_f^*.
3. The Q_f^* values for Aspartate and Glutamate rings are found to be different, and also to differ according to the ring's position along the SF. We connect this difference to the difference in protonation states between the EEEE and DDDD charged rings, which could depend on their radii. Another possibility [32] is that the EEEE and DDDD rings may be in different conformational states.
4. The zero-current Ca^{2+} ICB $Z_2 \approx -4e$ point was observed directly for the LDEWAS mutant, together with the $Z_1 \approx -2e$ point for LESWAS, and with the resonant conduction point $M_1 \approx -3e$ for LEDWAS lying between them. These results can be regarded as the first experimental observation of an ICB oscillation in biological ion channels, *cf.* the recent report of ICB in artificial sub-nm nanopores [23].
5. Our preliminary study of the effects of extracellular pH in the 6.4-8.4 range on Ca^{2+} conductance confirms our attribution of the Ca^{2+} Z_1 ICB blockade point for LESWAS, whereas the LDSWAS behaviour does not fit the scheme and clearly requires farther investigation.

The overall conclusion is that, allowing for possible protonation, the ICB/QD model provides a good description of most features of the conduction and selectivity of the NaChBac channel and its mutants. The model could also be applicable to other biological ion channels and to artificial nanopores.

Authors Contributions

OAF: Experimental design, conducting experiments, text writing and editing, data analysis.
IKK: Experimental design, model development, text writing and editing, data analysis.
WATG: Model development, data analysis
MLB Brownian dynamics simulations for parametric testing of ICB model
DGL: Model development, data analysis
SKR: Experimental design, data analysis, text writing and editing
PVEMcC: Model development, data analysis, text writing and editing

Acknowledgements

We are grateful to R. S. Eisenberg, C. Guardiani, A. Stefanovska, and M. Di Ventra, for comments and useful discussions. We thank Huaping Sun, for her much appreciated help with the generation of mutant channels. The research was supported by the Engineering and Physical Sciences Research Council UK [grant No. EP/M015831/1] and by a Leverhulme Trust Research Project Grant RPG-2017-134.

Appendix A. Supplementary material

Supplementary Material for this article is available online at *** [PLEASE ADD LINK]

Appendix B. Supplementary data

Supplementary Material for this article is available online at

`https://dx.doi.org/10.17635/lancaster/researchdata/329`

References

[1] B. Hille, Ion Channels Of Excitable Membranes, 3rd Edition, Sinauer Associates, Sunderland, MA, 2001.

[2] G. Eisenman, R. Horn, Ionic selectivity revisited: the role of kinetic and equilibrium processes in ion permeation through channels, J. Membr. Biol. 76 (3) (1983) 197–225.

[3] A. Laio, V. Torre, Physical origin of selectivity in ionic channels of biological membranes, Biophys. J. 76 (1) (1999) 129–148.

[4] S. Bernèche, B. Roux, Energetics of ion conduction through the K^+ channel, Nature 414 (6859) (2001) 73–77.

[5] B. Nadler, U. Hollerbach, R. S. Eisenberg, Dielectric boundary force and its crucial role in gramicidin, Phys. Rev. E 68 (2, Part 1) (2003) 021905.

[6] T. W. Allen, O. S. Andersen, B. Roux, Energetics of ion conduction through the gramicidin channel, Proc. Nat. Acad. Sci. (USA) 101 (1) (2004) 117–122.

[7] S. O. Yesylevskyy, V. N. Kharkyanen, Barrier-less knock-on conduction in ion channels: peculiarity or general mechanism?, Chem. Phys. 312 (2005) 127–133.

[8] B. Corry, Mechanisms of selective ion transport and salt rejection in carbon nanostructures, MRS Bull. 42 (4) (2017) 306–310.

[9] A. M. Woodhull, Ionic blockage of sodium channels in nerve, J. Gen. Physiol. 61 (6) (1973) 687–708.

[10] W. A. Sather, E. W. McCleskey, Permeation and selectivity in calcium channels, Ann. Rev. Physiol. 65 (2003) 133–159.

[11] D. Gillespie, D. Boda, The anomalous mole fraction effect in calcium channels: A measure of preferential selectivity, Biophys. J. 95 (2008) 2658–2672.

[12] M. Krems, M. Di Ventra, Ionic Coulomb blockade in nanopores, J. Phys. Condens. Matter 25 (2013) 065101.

[13] I. K. Kaufman, P. V. E. McClintock, R. S. Eisenberg, Coulomb blockade model of permeation and selectivity in biological ion channels, New J. Phys. 17 (8) (2015) 083021.

[14] I. K. Kaufman, W. A. T. Gibby, D. G. Luchinsky, P. V. E. McClintock, R. S. Eisenberg, Coulomb blockade oscillations in biological ion channels, in: Proc. 23rd Intern. Conf. on Noise and Fluctuations (ICNF), Xian, IEEE Conf. Proc., 2015, p. doi: 10.1109/ICNF.2015.7288558. doi:10.1109/ICNF.2015.7288558.

[15] E. Kitzing, A novel model for saturation of ion conductivity in transmembrane channels, in: A. Pullman, J. Jortner, B. Pullman (Eds.), Membrane Proteins: Structures, Interactions and Models: Proceedings of the Twenty-Fifth Jerusalem Symposium on Quantum Chemistry and Biochemistry, Jerusalem, Israel, May 18-21,1992, Springer Netherlands, Dordrecht, 1992, pp. 297–314.

[16] J. Zhang, A. Kamenev, B. I. Shklovskii, Conductance of ion channels and nanopores with charged walls: A toy model, Phys. Rev. Lett. 95 (14) (2005) 148101.

[17] I. K. Kaufman, D. G. Luchinsky, R. Tindjong, P. V. E. McClintock, R. S. Eisenberg, Multi-ion conduction bands in a simple model of calcium ion channels, Phys. Biol. 10 (2) (2013) 026007.

[18] I. K. Kaufman, D. G. Luchinsky, R. Tindjong, P. V. E. McClintock, R. S. Eisenberg, Energetics of discrete selectivity bands and mutation-induced transitions in the calcium-sodium ion channels family, Phys. Rev. E 88 (5) (2013) 052712.

[19] P. Läuger, Ion transport through pores: A rate-theory analysis, BBA – Biomembranes 311 (3) (1973) 423–441.

[20] D. V. Averin, K. K. Likharev, Coulomb blockade of single-electron tunneling, and coherent oscillations in small tunnel junctions, J. Low Temp. Phys. 62 (3-4) (1986) 345–373.

[21] C. W. J. Beenakker, Theory of Coulomb-blockade oscillations in the conductance of a quantum dot, Phys. Rev. B 44 (4) (1991) 1646–1656.

[22] H. Grabert, M. H. Devoret, Single Charge Tunneling: Coulomb Blockade Phenomena in Nanostructures, Vol. 294, Springer Science & Business Media, 2013.

[23] J. Feng, K. Liu, M. Graf, D. Dumcenco, A. Kis, M. Di Ventra, A. Radenovic, Observation of ionic Coulomb blockade in nanopores, Nature Mater. 15 (8) (2016) 850 – 855.

[24] I. K. Kaufman, W. A. T. Gibby, D. G. Luchinsky, P. V. E. McClintock, Effect of local binding on stochastic transport in ion channels, in: 2017 Intern. Conf. on Noise and Fluctuations 10.1109/ICNF.2017.7985974, 2017, pp. 1–4. doi:10.1109/ICNF.2017.7985974.

[25] D. G. Luchinsky, W. A. T. Gibby, I. K. Kaufman, P. V. E. McClintock, D. A. Timucin, Relation between selectivity and conductivity in narrow ion channels, in: 2017 International Conference on Noise and Fluctuations (ICNF), 2017, p. DOI: 10.1109/ICNF.2017.7985973. doi:10.1109/ICNF.2017.7985973.

[26] I. K. Kaufman, O. A. Fedorenko, D. G. Luchinsky, W. A. T. Gibby, S. K. Roberts, P. V. E. McClintock, R. S. Eisenberg, Ionic Coulomb blockade and anomalous mole fraction effect in the NaCh
EPJ Nonlin. Biomed. Phys. 5 (2017) 1–8. doi:10.1051/epjnbp/2017003.
URL https://doi.org/10.1051/epjnbp/2017003

[27] D. J. Ren, B. Navarro, H. X. Xu, L. X. Yue, Q. Shi, D. E. Clapham, A prokaryotic voltage-gated sodium channel, Science 294 (5550) (2001) 2372–2375.

[28] L. X. Yue, B. Navarro, D. J. Ren, A. Ramos, D. E. Clapham, The cation selectivity filter of the bacterial sodium channel, NaChBac, J. Gen. Physiol. 120 (6) (2002) 845–853.

[29] P. G. DeCaen, Y. Takahashi, T. A. Krulwich, M. Ito, D. E. Clapham, Ionic selectivity and thermal adaptations within the voltage-gated sodium channel family of alkaliphilic Bacillus, eLife 3 (2014) e04387.

[30] R. K. Finol-Urdaneta, Y. Wang, A. Al-Sabi, C. Zhao, S. Y. Noskov, R. J. French, Sodium channel selectivity and conduction: prokaryotes have devised their own molecular strategy, J. Gen. Physiol. 143 (2) (2014) 157–171.

[31] C. E. Naylor, C. Bagnéris, P. G. DeCaen, A. Sula, A. Scaglione, D. E. Clapham, B. A. Wallace, Molecular basis of ion permeability in a voltage-gated sodium channel, EMBO J. 35 (8) (2016) 820–830. doi:10.15252/embj.201593285.

[32] C. Guardiani, P. M. Rodger, O. A. Fedorenko, S. K. Roberts, I. A. Khovanov, Sodium binding sites and permeation mechanism in the NaChBac channel: A molecular dynamics study, J. Chem. Theor. Comput. 13 (2017) 1389–1400. doi:10.1021/acs.jctc.6b01035.

[33] C. Guardiani, O. A. Fedorenko, S. K. Roberts, I. A. Khovanov, On the selectivity of the NaChBac channel: an integrated computational and experimental analysis of sodium and calcium permeation, Phys. Chem. Chem. Phys. 19 (2017) 29840–29854. doi:10.1039/C7CP05928K.

[34] W. A. Catterall, G. Wisedchaisri, N. Zheng, The chemical basis for electrical signaling, Nature Chem. Biol. 13 (5) (2017) 455–463.

[35] J. Payandeh, D. L. Minor, Bacterial voltage-gated sodium channels (BacNaVs) from the soil, sea, and salt lakes enlighten molecular mechanisms of electrical signaling and pharmacology in the brain and heart, J. Mol. Biol. 427 (1) (2015) 3–30.

[36] R. S. Eisenberg, Ionic channels in biological membranes – electrostatic analysis of a natural nanotube, Contemp. Phys, 39 (1998) 447–466.

[37] J. Zhang, B. I. Shklovskii, Effective charge and free energy of DNA inside an ion channel, Phys. Rev. E 75 (2) (2007) 021906.

[38] M. Aguilella-Arzo, J. J. García-Celma, J. Cervera, A. Alcaraz, V. M. Aguilella, Electrostatic properties and macroscopic electrodiffusion in OmpF porin and mutants, Bioelectrochem. 70 (2) (2007) 320–327.

[39] X.-H. Chen, R. W. Tsien, Aspartate substitutions establish the concerted action of P-region glutamates in repeats I and III in forming the protonation site of L-type Ca^{2+} channels, J. Biol. Chem. 272 (48) (1997) 30002–30008.

[40] G. Job, R. Rüffler, Physical Chemistry from a Different Angle, Springer, 2016.

[41] P. Beroza, D. R. Fredkin, M. Y. Okamura, G. Feher, Protonation of interacting residues in a protein by a Monte Carlo method: application to lysozyme and the photosynthetic reaction center of Rhodobacter sphaeroides., Proc. Nat. Acad. Sci.

(USA) 88 (13) (1991) 5804–5808.
[42] S. Furini, P. Barbini, C. Domene, Effects of the protonation state of the EEEE motif of a bacterial Na^+-channel on conduction and pore structure, Biophys. J. 106 (2014) 2175–2183.
[43] B. Roux, T. Allen, S. Berneche, W. Im, Theoretical and computational models of biological ion channels, Quart. Rev. Biophys. 37 (1) (2004) 15–103.
[44] B. Corry, T. W. Allen, S. Kuyucak, S. H. Chung, Mechanisms of permeation and selectivity in calcium channels, Biophys. J. 80 (1) (2001) 195–214.
[45] D. Boda, W. Nonner, D. Henderson, B. Eisenberg, D. Gillespie, Volume exclusion in calcium selective channels, Biophys. J. 94 (9) (2008) 3486–3496.
[46] W. Nonner, B. Eisenberg, Ion permeation and glutamate residues linked by Poisson-Nernst-Planck theory in L-type calcium channels, Biophys. J. 75 (3) (1998) 1287–1305.
[47] I. K. Kaufman, W. A. T. Gibby, D. G. Luchinsky, P. V. E. McClintock, Effect of local binding on stochastic transport in ion channels, arXiv preprint arXiv:1704.00956 (2017).
[48] S. Sahu, M. Di Ventra, M. Zwolak, Dehydration as a universal mechanism for ion selectivity in graphene and other atomically thin pores, Nano Lett. 17 (8) (2017) 4719–4724.
[49] K. Li, Y. Tao, Z. Li, J. Sha, Y. Chen, Selective ion-permeation through strained and charged graphene membranes, Nanotech. 29 (3) (2017) 035402.
[50] M. Zwolak, J. Lagerqvist, M. Di Ventra, Quantized ionic conductance in nanopores, Phys. Rev. Lett. 103 (2009) 128102.
[51] C. Boiteux, E. Flood, T. W. Allen, Comparison of permeation mechanisms in sodium-selective ion channels, Neurosci. Lett. DOI: 10.1016/j.neulet.2018.05.036 (2018) 1–6.
[52] L. Tang, T. M. G. El-Din, J. Payandeh, G. Q. Martinez, T. M. Heard, T. Scheuer, N. Zheng, W. A. Catterall, Structural basis for Ca^{2+} selectivity of a voltage-gated calcium channel, Nature 505 (7481) (2014) 56–61.
[53] R. E. Kirk, Experimental Design, Wiley Online Library, 1982.
[54] T. Vora, B. Corry, S. Chung, Brownian dynamics study of flux ratios in sodium channels, Eur. Biophys. J. 38 (1) (2008) 45–52.
[55] Y. B. Wang, R. K. Finol-Urdaneta, V. A. Ngo, R. J. French, S. Y. Noskov, Bases of bacterial sodium channel selectivity among organic cations, Sci. Rep. 9 (2019) 18992.
[56] C. Guardiani, O. A. Fedorenko, I. A. Khovanov, S. K. Roberts, Different roles for aspartates and glutamates for cation permeation in bacterial sodium channels, BBA-Biomembranes 1861 (2019) 495–503.
[57] D. Gillespie, Energetics of divalent selectivity in a calcium channel: The ryanodine receptor case study, Biophys. J. 94 (4) (2008) 1169–1184.
[58] P. T. Ellinor, J. Yang, W. A. Sather, J.-F. Zhang, R. W. Tsien, Ca^{2+} channel selectivity at a single locus for high-affinity Ca^{2+} interactions, Neuron 15 (5) (1995) 1121–1132.
[59] D. P. Lotshaw, K. A. Sheehan, Divalent cation permeability and blockade of Ca^{2+}-permeant non-selective cation channels in rat adrenal zona glomerulosa cells, J. Physiol. 514 (2) (1999) 397–411.
[60] S. Bernèche, B. Roux, The ionization state and the conformation of Glu-71 in the KcsA K^+ channel, Biophys. J. 82 (2) (2002) 772–780. doi:https://doi.org/10.1016/S0006-3495(02)75439-8.
[61] B. Corry, M. Thomas, Mechanism of ion permeation and selectivity in a voltage gated sodium channel, J. Amer. Chem. Soc. 134 (3) (2012) 1840–1846.